Applied Catalysis B: Environmental 160–161 (2014) 374–382

Contents lists available at ScienceDirect

Applied Catalysis B: Environmental

journal homepage: www.elsevier.com/locate/apcatb

Mixed-phase TiO_2 photocatalysts: Crystalline phase isolation and reconstruction, characterization and photocatalytic activity in the oxidation of 4-chlorophenol from aqueous effluents

Petru Apopei[a], Cezar Catrinescu[a,*], Carmen Teodosiu[a], Sébastien Royer[b]

[a] "Gheorghe Asachi" Technical University of Iasi, Faculty of Chemical Engineering and Environmental Protection Department of Environmental Engineering and Management, 73 Prof. dr. docent Dimitrie Mangeron Street, 700050 Iasi, Romania
[b] Université de Poitiers, CNRS UMR 7285, IC2MP, 4 rue Michel Brunet, 86022 Poitiers Cedex, France

ARTICLE INFO

Article history:
Received 13 March 2014
Received in revised form 5 May 2014
Accepted 18 May 2014
Available online 27 May 2014

Keywords:
4-Chlorophenol oxidation
Photocatalysis
Titanium dioxide
Band gap

ABSTRACT

Anatase and rutile isolated from Degussa P25 and two other TiO_2 commercial samples were used as starting materials for the preparation of different anatase/rutile physical mixtures for the photocatalytic oxidation of 4-chlorophenol from aqueous effluents. Degussa P25 was also used as reference active material. The samples were characterized by X-ray diffraction, nitrogen physisorption, Raman spectroscopy, high-resolution transmission electron microscopy and diffuse reflectance UV–vis spectroscopy. A special attention was given to the determination of the band gap energy, by using two methods: Tauc plots and derivative spectroscopy. The second method seems more accurate, eliminating a certain degree of subjectivity, inherent to the Tauc-plot method. The photocatalytic tests showed that Degussa P25 was the most active photocatalyst, followed closely by anatase separated from Degussa P25 and by commercial anatase. The addition of rutile to the anatase powder produced a decrease in the photocatalytic activity. The photocatalytic tests showed that the original Degussa P25 was more active than the anatase phase from its composition, which in turn performed better than the reconstructed P25 in the photocatalytic test given an evidence that the supposed synergistic effect does not operate in this particular case.

1. Introduction

Heterogeneous photocatalysis on semiconductor powders is recognized as a viable advanced oxidation process (AOP) for the degradation of priority organic pollutants from wastewaters. Photocatalysis is usually described as the process in which a chemical reaction is induced when a semiconductor, which acts as a photocatalyst, is irradiated with photons of energy higher than or equal to its band gap energy, to produce photo-electrons and photo-holes [1,2]. During a photocatalytic reaction, reactants can be adsorbed and react with either photo-electrons (acceptor molecules like dissolved O_2) or with the photo-holes (donor molecules like H_2O, for example) to produce oxidizing species like superoxide radical anion or hydroxyl radical, respectively, which consequently will oxidize pollutant species [2].

Applications of photocatalysis in this field are determined by the characteristics (composition, flow, etc.) of the aqueous influents that are processed and the quality requirements for the treated effluent. Among many candidates for photocatalysts, TiO_2 is almost the only material suitable for industrial use to date and also probably in the future [3].

TiO_2 exhibits three distinct polymorphs (anatase, rutile and brookite) of which only anatase, with a band gap of 3.2 eV, is functional as photocatalyst. Although rutile exhibits an energy band gap of only 3.02 eV, its photocatalytic activity in oxidation processes remains very low. Mixed-phase titania photocatalysts, containing both anatase and rutile crystallites, have been reported to display enhanced photoactivity relative to single-phase titania. For example, Degussa (Evonik) P25, Aeroxide TiO_2 P25, used as a de facto standard in photocatalysis by titania [4], is a mixed-phase titania photocatalyst. Moreover, this was the first paper discussing the photocatalytic activity of anatase and rutile particles separated from P25 as well as the synergetic effect of co-presence of anatase and rutile. The reason for this so-called synergistic effect is still not fully elucidated although some speculative explanations have been proposed. An improved charge carrier separation, possibly through the trapping of electrons in rutile and the consequent reduction in electron–hole recombination [5–7] is usually invoked to explain

* Corresponding author. Tel.: +40 232 237594; fax: +40 232 237594.
E-mail addresses: ccatrine@ch.tuiasi.ro, ccatrine@uma.pt (C. Catrinescu).

http://dx.doi.org/10.1016/j.apcatb.2014.05.030
0926-3373/

this behavior. Surface trapping of holes together with lattice trapping of electrons has also been reported [8,9]. However, in order to check the synergistic effect of an anatase–rutile mixture such as Degussa P25, it is necessary to isolate anatase and rutile crystallites from the original material and to reconstruct it, by preparing physical mixtures of known phase compositions. Separation of rutile by selective dissolution of anatase from Degussa P25 in HF has been reported by Ohno et al. [10] Recently, Ohtani et al. [11] proposed a route to isolate anatase by selective dissolution of rutile from Degussa P25, by using a mixed solution of hydrogen peroxide and ammonia. These authors used these phases as standards for the calibration curves in the XRD, in order to calculate the precise crystalline composition of P25.

The first aim of this study is to validate the phase separation methods from Degussa P25 and to provide a thorough characterization of the isolated phases and of the reconstructed TiO_2 powders, following the works of Ohtani et al. [4,11]. Another objective of this research is to check the existence of the synergistic effect between anatase and rutile by studying the effect of the crystalline phase composition of different TiO_2 physical mixtures. Anatase and rutile phases, isolated from Degussa P25 or from commercial sources, were mixed and tested in the photocatalytic oxidation of 4-chlorophenol.

Chlorophenols represent common priority organic pollutants in water discharged by several industries and have particularities that make them useful model pollutants. Their properties, such as: toxicity (even at low concentrations), formation of substituted compounds during disinfection and oxidation processes (such as those used currently for the treatment of natural surface water for drinking purposes), phytotoxicity and ability to bioaccumulate in organisms, have similarities with other persistent organic pollutants. 4-chlorophenol, in particular, is considered a representative model of priority pollutants in water [12,13].

Finally, the possibility to replace the rather expensive Degussa P25 photocatalyst with other lower-price commercially available TiO_2 powders (eventually with larger crystal sizes to facilitate material recovering [14,15], was also studied. In this sense, the critical question to be answered is whether pure anatase should be used alone or the addition of rutile could enhance the photocatalytic activity of the material in the oxidation of priority organic pollutants from water.

2. Experimental

2.1. Materials

Three TiO_2 samples, from Sigma-Aldrich, were used in this study: anatase (denoted as An, product no. 232033), rutile (denoted as Ru, product no. 204757) and Degussa (Evronik) P25 (denoted as P25, product no.718467). The organic compound (4-chlorophenol, 4-CP) used for photocatalytic activity tests and the reagents used in phenol analysis (4-aminoantipyrine, potassium ferricyanide(III) and the ammonium chloride/ammonium hydroxide) were also supplied by Sigma-Aldrich.

2.2. Crystalline phase separation

Isolation of anatase powder from Degussa P25 was achieved by adopting the method described by Ohtani et al. [11]. The material issued from this treatment is denoted as An(P25). The method involves the dissolution of only the rutile phase from 0.5 g Degussa P25 in 50 mL of hydrogen peroxide (30%), and 5 mL ammonium hydroxide (2.5%). The precipitate obtained is isolated by centrifuging at 10,000 rpm for at least 5 min and is repeatedly washed with demineralized water. The powder obtained is dried and held at room temperature before use.

Rutile separation from commercial Degussa P25 composition was achieved by treatment with HF solution, conditions under which there is selective dissolution of anatase particles [10]. The material issued from this treatment is denoted as Ru(P25). The method involves the treatment of 2 g of commercial TiO_2 (Degussa P25) with 100 mL 10% HF solution. The suspension formed was stirred (500 rpm) for 24 h at room temperature. The solid is recovered by centrifugation or filtration. In order to eliminate fluoride ions (F^-) present in the media, the obtained solid was washed repeatedly with deionized water. The resulting solid (rutile) is dried for 2 h at 50 °C.

2.3. Characteristics of the photocatalytic materials

The photocatalyst samples were characterized using a Shimadzu UV-2450 spectrophotometer equipped with an integrating sphere (ISR-2200). The crystalline phase compositions of the samples were characterized by X-ray analysis using a Siemens D500 diffractometer. The recording was done on the field 6°–80° (2θ) by step of 0.02° (2θ) and a counting time of 23 s per step.

Raman spectra (Stokes spectra) were obtained at room temperature, using an HR UV 800 confocal scanning spectrometer (Horiba Jobin Yvon) equipped with a Peltier-cooled charge coupled device (1152 × 298 pixel) used for detection. The Raman scattering is excited using a 514.52 nm excitation wavelength supplied by an external, air-cooled, Ar^+ laser (Melles Griot) through an Olympus high-stability BXFM microscope coupled confocally.

The morphology of the powders was determined on a JEOL 2100 instrument, operated at 200 kV with a LaB6 source and equipped with a Gatan Ultra scan camera.

Nitrogen adsorption measurements were carried out at −196 °C with an automatic Micromeritics ASAP 2000 instrument.

2.4. Photocatalytic tests

In order to compare the photocatalytic activity of Degussa P25, pure rutile, pure anatase and different physical mixtures of these phases (3:1 anatase to rutile weight ratios), a photoreactor equipped with a 9 W UV-A immersion lamp, magnetic stirrer and air bubbling, has been used. The spectral response of lamp ranges between 350 and 400 nm, with a maximum at 366 nm. The initial light flux, as determined by chemical actinometry using potassium ferrioxalate, was 1.25×10^{-4} E min^{-1}.

The TiO_2 powder (200 mg L^{-1}) was dispersed in 500 mL aqueous solution containing 4-CP (20 mg L^{-1}) and stirred for 2 h under dark. Then, the UV lamp was turned on and the reaction was performed for 2 h. The 4-CP concentrations were analyzed by 4-aminoantypirine standard method, using a JASCO V-530 spectrophotometer.

3. Results and discussion

The XRD patterns of the three commercial TiO_2 powders are presented in Fig. 1A. The anatase phase was identified by the presence of intense diffraction peaks located at 25° and 48° while in the rutile phase the main peaks appeared at 27°, 36° and 55°. Although An and Ru are commercialized as pure anatase and rutile type materials, both are contaminated with small amounts of the other crystalline polymorph. A rough estimation, based on the intensities of the anatase (1 0 1) and rutile (1 1 0) XRD peaks, shows less than 1% impurity in both these samples. The coexistence of anatase and rutile phases in Degussa P25 sample is also confirmed by XRD analysis. It is known from literature that Degussa P25 is a mixture of anatase and rutile at proportions of 78% anatase, 14% rutile and 8%

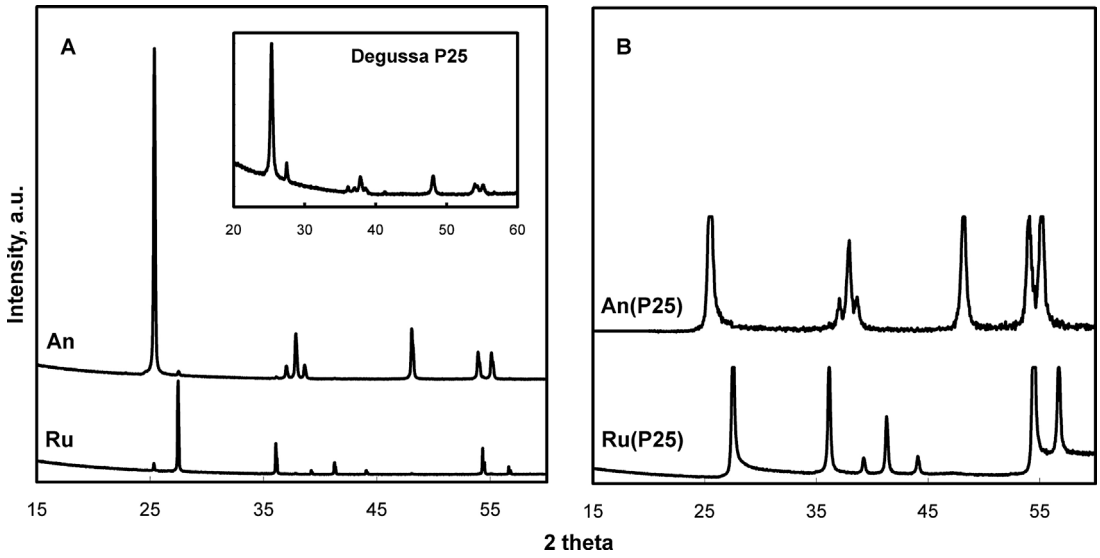

Fig. 1. XRD normalized patterns recorded for (A) P25, An, Ru and (B) An(P25) and Ru(P25)materials.

Table 1
Crystallite size and surface area of the photocatalysts.

Sample	D (nm)	S_{BET} ($m^2\ g^{-1}$)
P25	39.5 (anatase), 58.2 (rutile)	57.3
An	95.2	11.9
An(P25)	41.5	64.2
Ru	–	3.5
Ru(P25)	65	39.8

amorphous TiO_2 (wt.) [8,16–18]. Well defined, narrow and intense diffraction peaks are observed for An and Ru, while Degussa P25 displays less intense and broad peaks for both anatase and rutile phases. This is due to the smaller size of the particles coexisting in Degussa P25 as compared with "pure" An and Ru samples.

The diffraction patterns of anatase (An(P25)) and rutile (Ru(P25)) separated from P25 are shown in Fig. 1B. The absence of any contamination with the other crystalline phase confirmed the viability of these selective dissolution methods To achieve XRD pure phase materials.

In addition, no significant change in the size of the crystallites (as estimated from the corrected FWHM of the reflections, by using the Scherrer equation) was noticed in the isolated phases, as compared to the original P25 (Table 1).

All samples display nitrogen adsorption–desorption isotherms of type II, with a narrow hysteresis at high partial pressures. B.E.T. surface areas are gathered in Table 1.

This shape of the adsorption–desorption isotherms is characteristic of non-porous materials, with the surface areas being mainly external and related to the size of the particles. The narrow hysteresis indicates the presence of intercrystalline mesoporosity. This is consistent with the morphological model proposed for Degussa P25, composed of agglomerates of crystallites with mesopores located between these agglomerates (inter-agglomerate pores). The specific surface area of An(P25) is slightly higher than that of the original P25. This seems reasonable because Ru, the other component of P25, has larger crystallites, with lower associated specific surface area.

TEM was used to further examine the particle size, crystallinity and morphology of the samples. TEM bright field images of different TiO_2 powders (An, Ru, An(P25), Ru(P25) and Degussa P25) are displayed in Figs. 4–6. It can be clearly observed that An shows mainly spherical-shaped and non-aggregated particles, while rutile consists in both spherical and rod shapes. The high crystallinity of anatase is indicated by clearly visible crystallographic fringes in Fig. 2B, corresponding to (1 0 1) plane with an interplanar distance of 0.343 nm. Furthermore, it can be estimated that particle size in An material is 100–300 nm for most of the particles (Fig. 2A), whereas the particle size in Ru material is about 0.3–1.5 μm (Fig. 2C).

TEM images of P25 powder (Fig. 3A and B), clearly indicate that anatase and rutile exist as separated particles and confirm that the average diameters of anatase and rutile particles are estimated to be around 30–40 and 60 nm, respectively [7].

The isolation methods do not significantly alter the morphology and the size of anatase (An(P25) material, Fig. 3C and D) and rutile (Ru(P25) material, Fig. 3E and F) particles. The high-resolution TEM (HRTEM) images show that the lattice fringes on the crystal faces have interplanar spacings of 3.47 Å (Fig. 3D) and 3.25 Å (Fig. 3F), corresponding to the (1 0 1) plane of anatase and to the (1 1 0) face of rutile, respectively.

Besides XRD, Raman spectroscopy was also used to distinguish the TiO_2 crystalline phases from the powder mixtures [19]. The anatase spectrum shows the presence of five characteristic Raman lines, observed at 143.9 cm^{-1} (E_g), 196.9 cm^{-1} (E_g), 395.9 cm^{-1} (B1g), 517.2 cm^{-1} (A1g + B1g), and 639.5 cm^{-1} (E_g) which can be assigned to the E_g, E_g, B1g, A1g + B1g and E_g Raman active fundamentals of TiO_2 anatase. The bands observed at 448 cm^{-1} and at 611.5 cm^{-1} are characteristic of the E_g and A1g modes of the rutile phase.

Fig. 4A presents the Raman spectra of the TiO_2 commercial samples. The presence of both TiO_2 crystalline phases for P25 is clearly confirmed by the spectrum recorded for this sample (Fig. 4A), as it contains all of the characteristic bands belonging to anatase and rutile phase. The spectrum of Ru displays, in addition to the typical bands of the rutile phase, a shoulder at 514 nm characteristic of the anatase phase. The spectrum recorded for the An sample displays only the characteristic bands of the anatase phase, although the presence of a small amount of rutile was also identified in the XRD pattern. Even if Raman spectroscopy is known to be very sensitive to the identification of various TiO_2 crystalline phases, in this particular case, it was not able to detect the presence of rutile traces in the commercial anatase sample.

The spectra of An(P25) and Ru(P25) (Fig. 4B) display only the characteristic bands for pure anatase and rutile, respectively, confirming the XRD data which show the production of pure isolated crystalline phases.

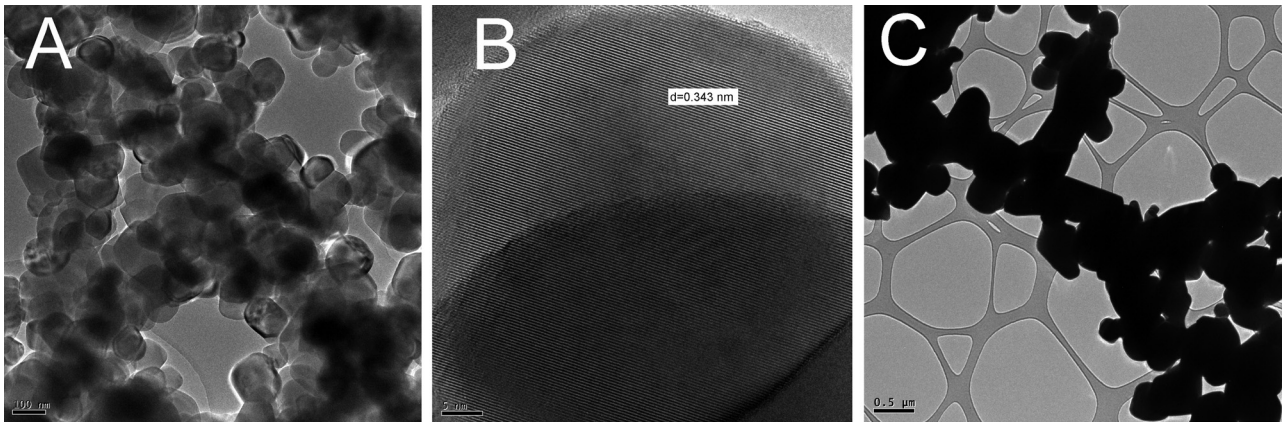

Fig. 2. Images of anatase and rutile commercial phases: ((A)–(B)) An sample; (C) Ru sample.

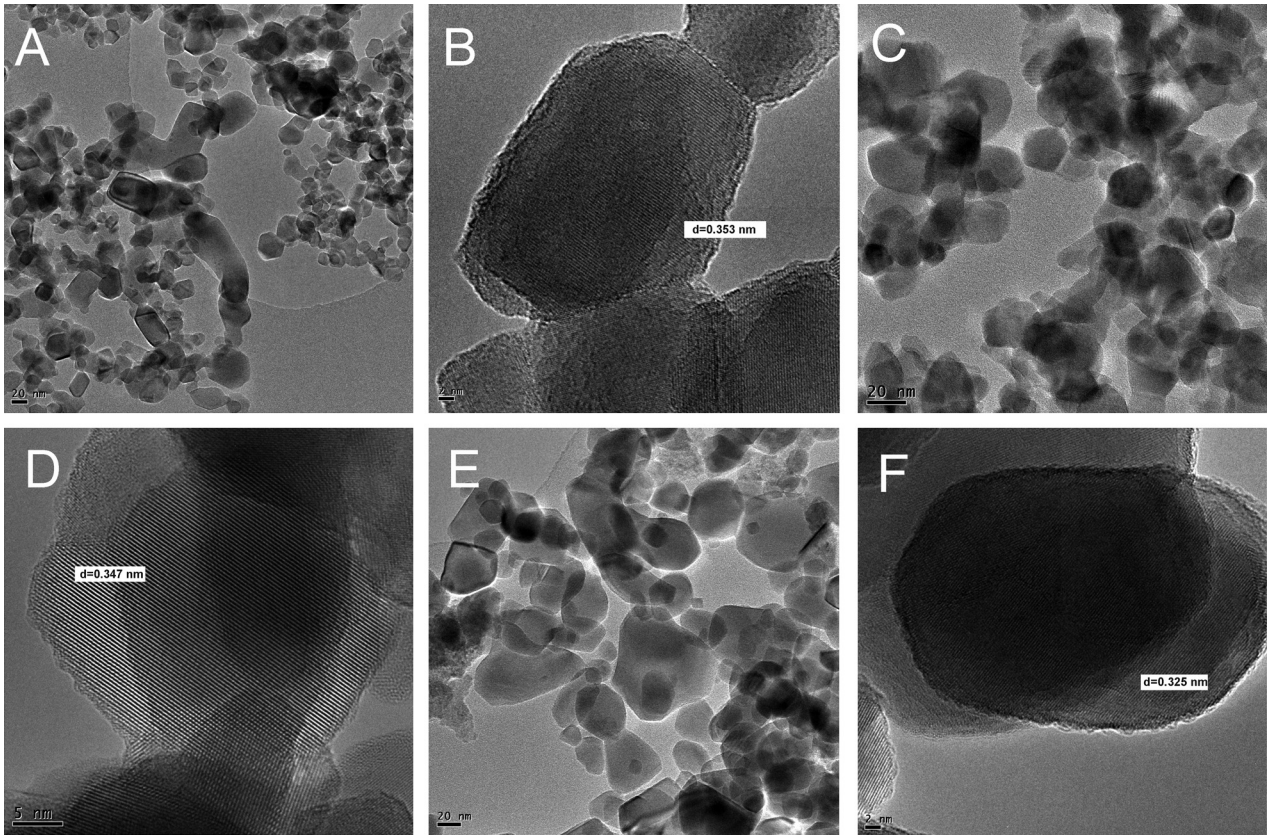

Fig. 3. Representative images recorded for: ((A)–(B)) Degussa P25 titania; ((C)–(D)) An(P25) and ((E)–(F)) Ru(P25) samples.

The band gap values of our TiO_2 samples were calculated from the DR UV–vis spectra displayed in Fig. 5.

An abrupt decrease in the reflectance coefficient that occurs within a narrow range of wavelengths (between 360 and 420 nm) is observed for all TiO_2 samples. This distinct edge of the optical reflectance may be correlated with the onset of the tail of the absorption curve and, in consequence, with the optical band gap. The wavelength at the inflexion point corresponds to E_g. It can be observed that the curve corresponding to rutile is shifted toward longer wavelengths with respect to anatase, confirming that rutile has a slightly narrower band-gap than anatase.

Two independent methods, differential diffuse reflectance spectral analysis and Tauc plot (based on Kubelka–Munk model), were used to calculate the forbidden band gap (E_g).

Optical band-gap could be estimated by using the following equation:

$$(\alpha\nu)^{1/n} = h\nu - E_g \quad (1)$$

where α, h, ν, E_g and n are absorption coefficient (α), Planck constant (h), wavenumber (ν), optical band-gap (E_g) and a constant (n) related to the transition mode. By verifying the linearity of plots $(\alpha\nu)^{1/n}$ as a function of $h\nu$ using n as 2 or 1/2, the mode of transition and the optical band-gap, as the x-intercept of the straight region of the curve, are estimated. Kubelka–Munk function was used instead the absorption coefficient of the TiO_2 powders, assuming that the scattering is constant over the used wavelength range.

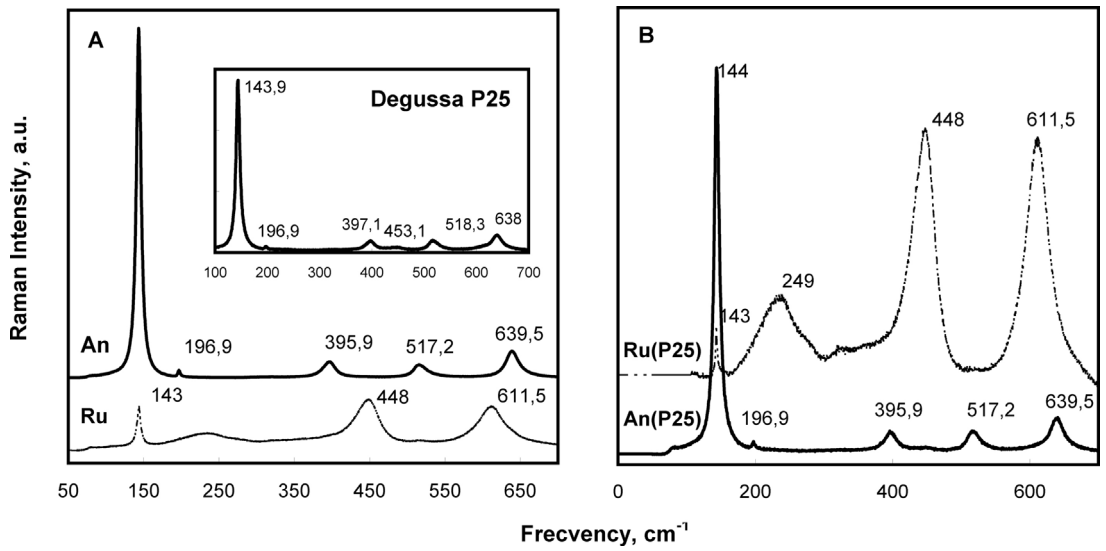

Fig. 4. Raman spectra of the: (A) An, Ru, Degussa P25 and (B) An (P25) and Ru (P25) materials.

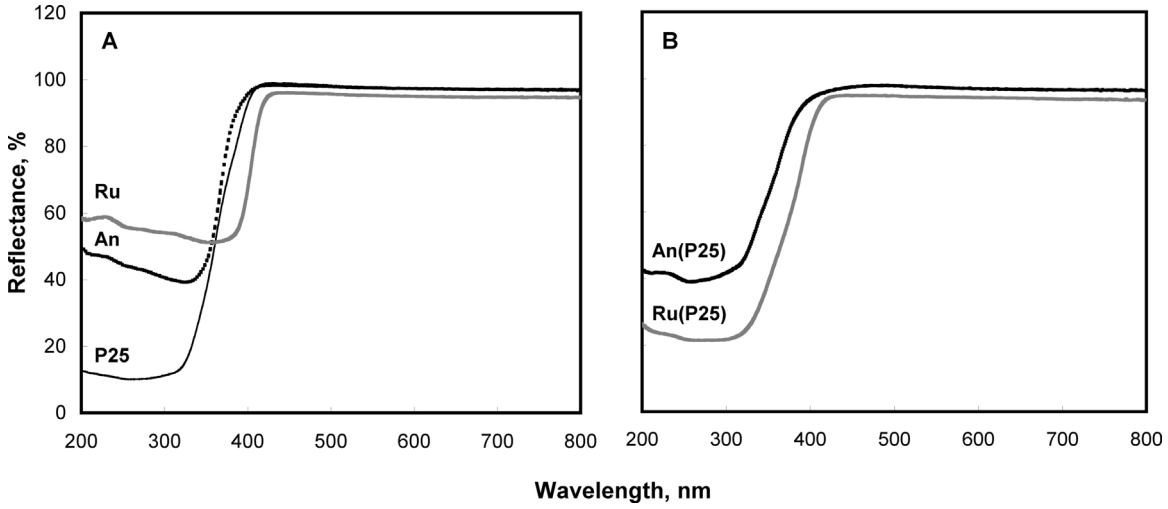

Fig. 5. DR UV–vis spectra of the: (A) TiO_2 commercial samples and (B) separated phases from Degussa P25.

The Kubelka–Munk transformation was applied to convert the diffuse reflectance measurements into the equivalent absorption coefficient, according to the following equation [20,21]:

$$K = \frac{(1-R)^2}{2R} \quad (2)$$

The obtained values were used for the construction of the Tauc plots for direct and indirect allowed transition (Figs. 6 and 7). The values of the band gap energies, derived from this method, are listed in Table 2.

From literature it is well known that rutile has both direct and indirect band-gaps (3.02–3.24 eV), whereas anatase exhibits only an indirect band-gap at 3.23–3.59 eV [22–24]. For anatase, we found an extrapolated band gap (absorbance level at zero or at background signal) in the indirect-allowed plot of absorbance of about 3.33 eV. In the case of rutile, independent of the plot type (i.e. square root or second power), extrapolated band gap values lie in the 3.0–3.15 eV range. Although these values are in accordance with the literature data, the use of Tauc plots for the determination of the band-gap energies has been recently criticized [25] in a review

Table 2
The band gap energies of photocatalysts.

Sample	Band gap (eV)			
	First derivative UV VIS/DR spectra		Tauc plot	
	Rutile	Anatase	Direct transition, $n = 1/2$	Indirect transition, $n = 2$
Degussa P25	3.17	3.43	3.28	3.2
An	3.1	3.38	3.41	3.33
An(P25)	–	3.43	3.34	3.25
Ru	3.07	3.35	3.13	3.07
Ru(P25)	3.17	–	3.15	3.01

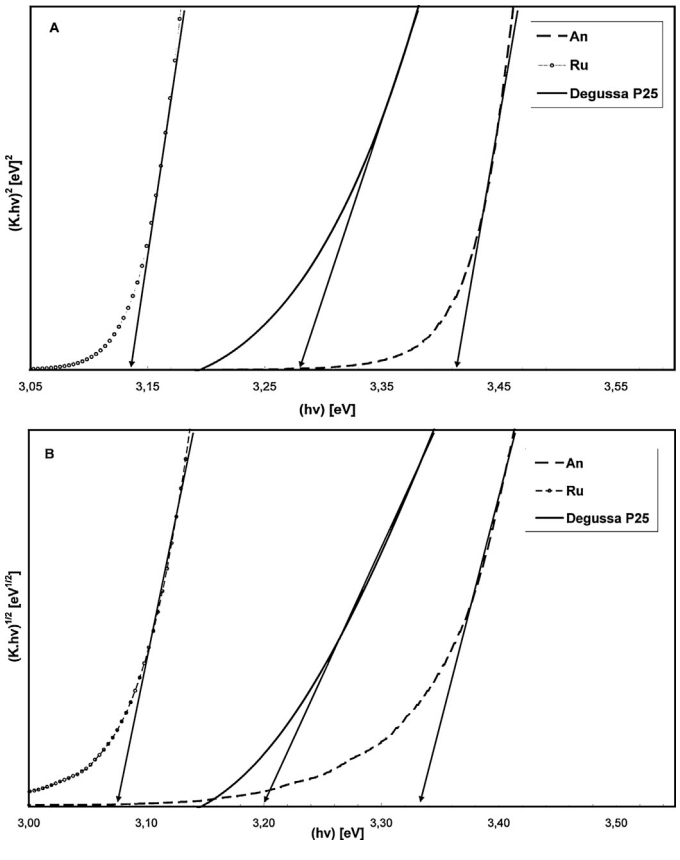

Fig. 6. The Tauc plots of An, Ru and P25 samples, calculated for different value of the power coefficient: $n = 1/2$ direct allowed (A), $n = 2$ indirect allowed (B) electronic transition.

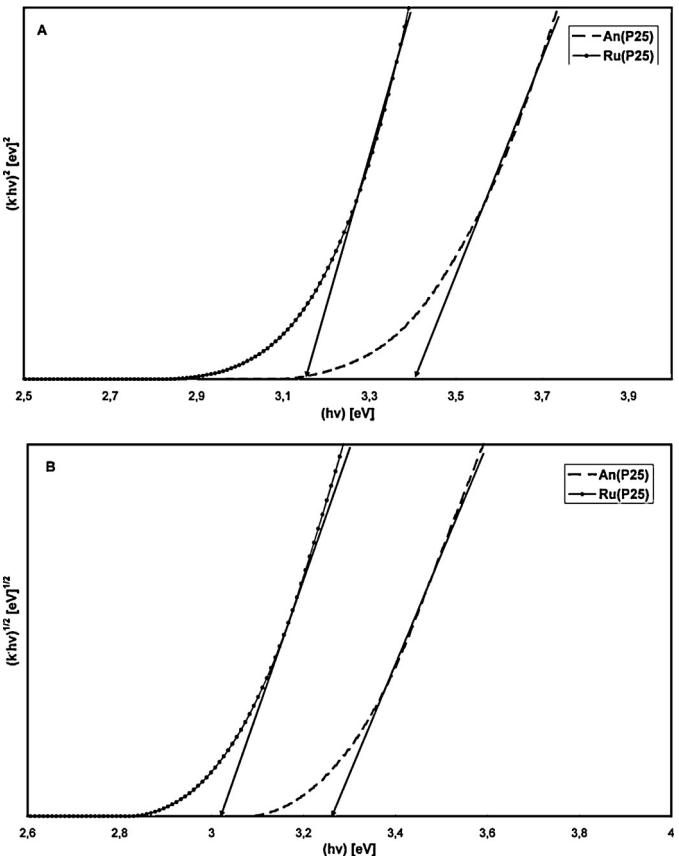

Fig. 7. The Tauc plots of the separated phases from Degussa P25: An (P25) and Ru (P25), calculated for different value of the power coefficient: $n = 1/2$ direct allowed (A), $n = 2$ indirect allowed (B) electronic transition.

article. According to this author, the choice of the linear part of the curve has a large degree of subjectivity, and there are no rules to discriminate a mode of transition on the basis of the range of the linear part. In addition, the interpretation is even more problematic with mixed-phase photocatalysts, such as P25.

A better alternative for the determination of the band gap energies would be to use a plot of the differential reflectance $dR/d\lambda$ as a function of λ, as presented in Fig. 8. The peaks at a certain wavelength correspond to the inflection point in the optical reflectance spectrum and thus to the band gap of the sample. An and Ru materials give rise apparently to single peaks, centered at 367 nm (3.38 eV) and 404 nm (3.07 eV), respectively. Samples consisting in a mixture of anatase and rutile, exhibit more complex signal. The deconvolution of the first derivative curves allowed a

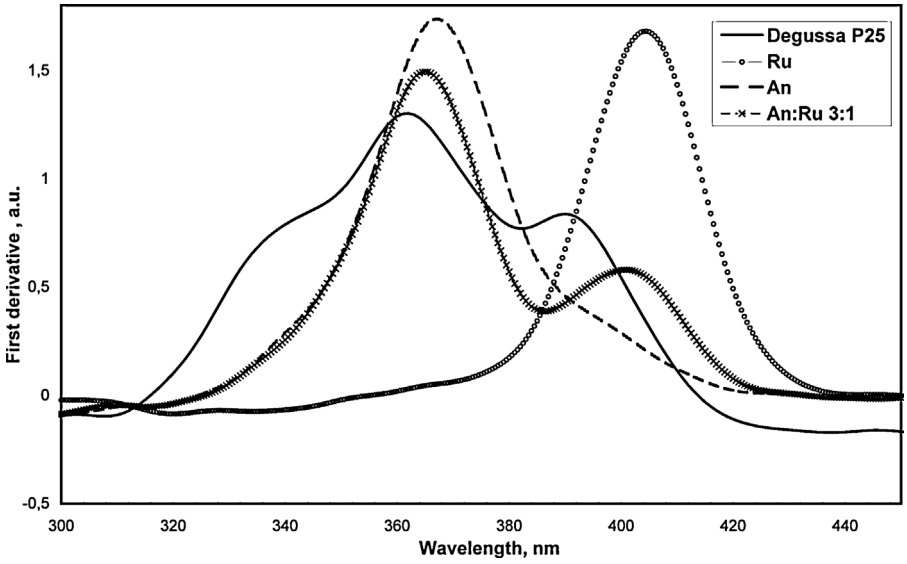

Fig. 8. First derivative obtained from UV–vis/DR spectra.

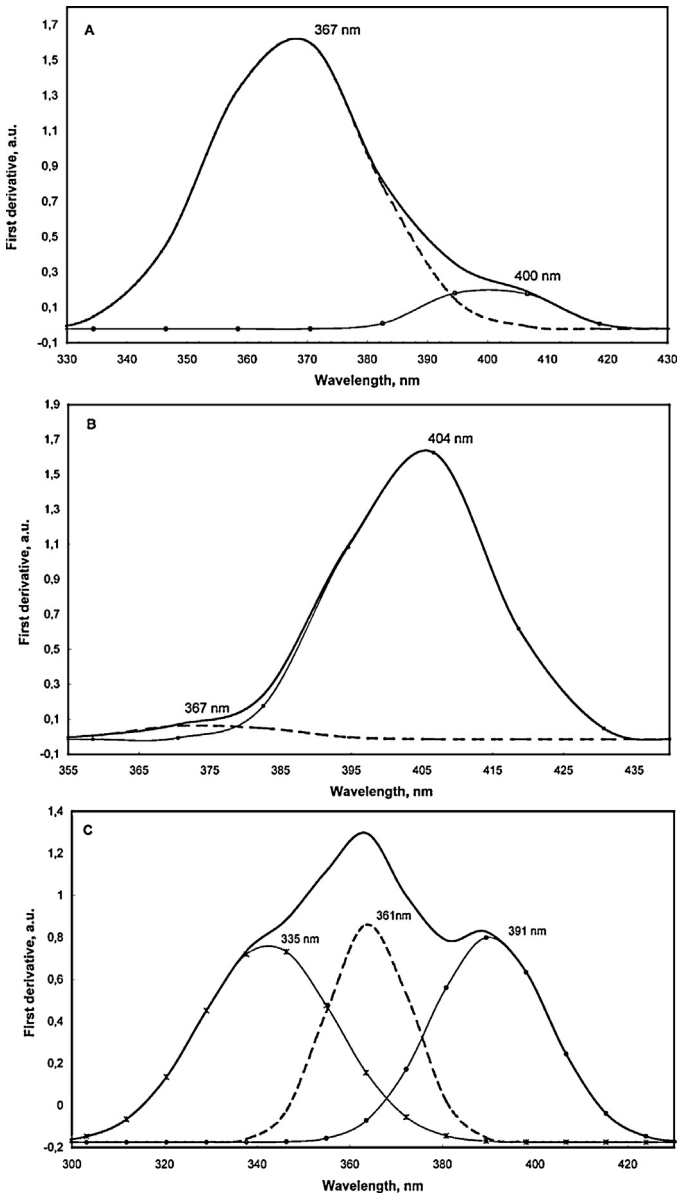

Fig. 9. The first derivative curve fitted with Gaussian peaks for (A) An sample, (B) Ru sample and (C) P25 sample.

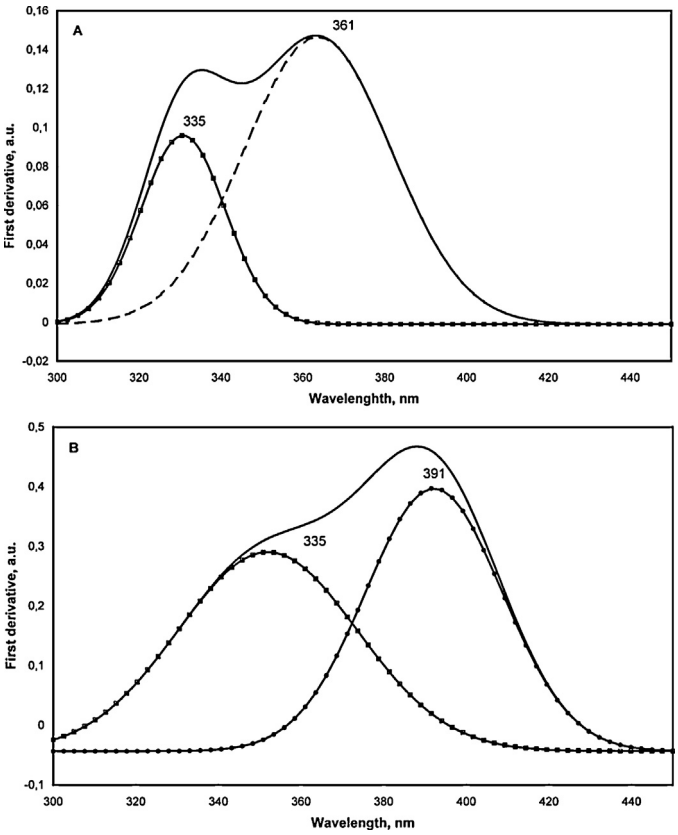

Fig. 10. The first derivative curve fitted with Gaussian peaks: (A) An(P25) and (B) Ru(P25).

more detailed interpretation of the spectra and a more accurate determination of the E_g values (Table 2).

The first derivative curve for An sample can be fitted with two Gaussian peaks (Fig. 9A), a major one, centered at 367 nm (3.38 eV), and a minor component at 400 nm (3.1 eV), that can be ascribed to anatase and rutile phases, respectively. This confirms the XRD and Raman data, which show the contamination of the "pure" An sample with some rutile phase. Similarly, a small peak at 367 nm was found in the curve corresponding to "pure" Ru (Fig. 9B), and was attributed to anatase phase. The physical mixture of An and Ru displays two well-defined peaks, located at the same positions as in the staring (original) phases. Degussa P25 exhibits a particular shape of the first derivative curve (Fig. 9C). First, the peak attributable to rutile appears shifted at 391 nm (3.17 eV). Then, in the 300–380 nm region, where the anatase peak usually appears, two peaks could be clearly observed. While the first one, at 361 nm (3.43 eV), could be ascribed to anatase, the second one, at 335 nm (3.7 eV), is more difficult to interpret. A similar observation was made by Chiarello et al. [26] for Degussa P25 and other anatase–rutile mixtures prepared by flame spray pyrolysis. The authors suggest that this signal could originate from the splitting of the anatase peak, due to a possible interaction between rutile and anatase crystals in strong contact. However, we did not observe comparable splitting in our physical mixtures (presented for An:Ru = 3:1 (wt.%), Fig. 8). In order to prove that the contact between TiO_2 phase leads to a change of the DR UV–vis spectrum, the physical mixtures were ultrasonicated for 30 min, supposing that after this treatment the smaller anatase crystals will be loaded on the larger rutile particles. Ohno et al. [7] showed that after sonication, the separated agglomerates of anatase and rutile particles are broken, and the phase get in close contact, leading to the hypothetical synergy effect. No band splitting was observed in the spectrum of our mixed sample. This suggests that the contact between the particles, assumed to be induced by US treatment, is not at the origin of the so-called band splitting. Another hypothesis is to ascribe the band at 335 nm to amorphous TiO_2. More detailed studies are now in progress to understand the origin of the band.

The curves derived from the spectra of An(P25) and Ru(P25) (Fig. 10A and B) display peaks at 391 nm, 361 nm and 335 nm, at the same wavelengths as rutile, anatase and the unknown phase, respectively, in the derivative spectra of the original P25 sample (Fig. 9C). There is virtually no shift in the values of the band-gap energies for anatase and rutile after the selective dissolution processes. The band at 335 nm could be attributed neither to rutile nor to anatase, because it is present in both phases isolated from P25.

The photocatalytic activity, expressed by means of the removal efficiencies of 4-CP, for different TiO_2 samples is presented in Figs. 11 and 12. A blank experiment (not shown), performed in the absence of any photocatalysts, showed the absence of photodegradation of 4-CP, under these reaction conditions.

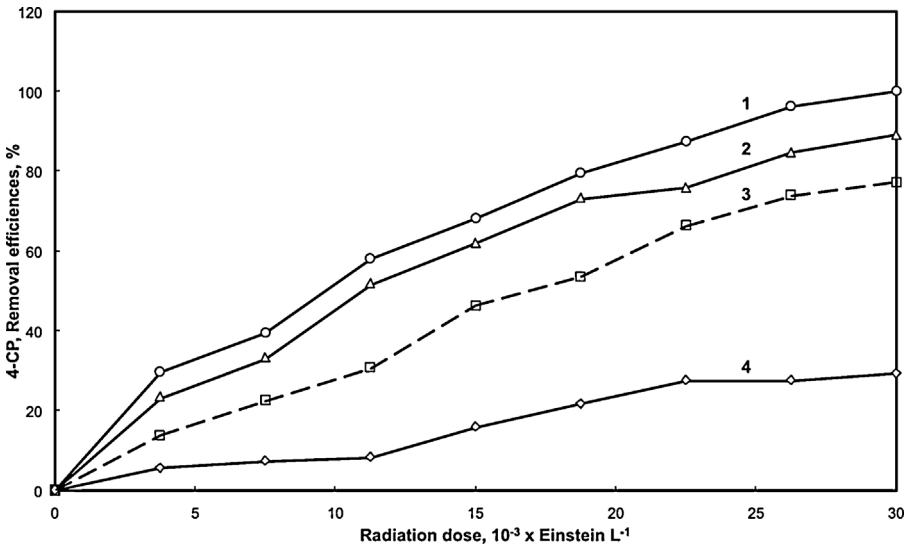

Fig. 11. 4-Chlorophenol removal efficiencies for commercial photocatalysts: (1) P25 sample, (2) An sample, (3) An:Ru = 3:1, (4) Ru sample, conditions: $T = 25\,^{\circ}C$, $V = 0.5\,L$, 500 rpm, pH = 5, $C_{4CP} = 20\,mg\,L^{-1}$; $C_{TiO_2} = 200\,mg\ L^{-1}\ ^{1}$ and time reaction = 120 min.

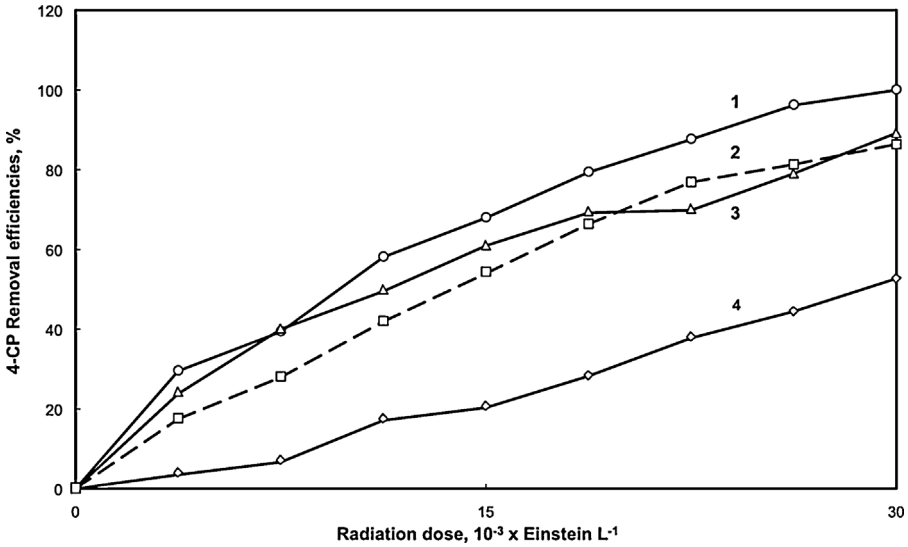

Fig. 12. 4-Chlorophenol removal efficiencies for separated photocatalysts: (1) P25 sample, (2) An(P25):Ru(P25) = 3:1, (3) An(P25), (4) Ru(P25), conditions: $T = 25\,^{\circ}C$, $V = 0.5\,L$, 500 rpm, pH = 5, $C_{4CP} = 20\,mg\,L^{-1}$; $C_{TiO_2} = 200\,mg\ L^{-1}$ and time reaction = 120 min.

Table 3
Comparison of 4-CP removal efficiencies for each photocatalyst.

Photocatalyst	Removal efficiency, (mmol 4-CP removed E^{-1})
Commercial samples and physical mixture	
P25	9.8
An	7.7
An:Ru = 3:1	4.8
Ru	1.7
Samples separated from P25 and reconstructed	
An(P25)	7.8
An(P25):Ru(P25) = 3:1	5.9
Ru(P25)	1.7

The 4-CP removal efficiency, calculated from the initial reaction rate and from the photon flux, for each photocatalyst tested, is listed in Table 3.

Table 3 Comparison of 4-CP removal efficiencies for each photocatalyst As expected, Degussa P25 is superior to the other single or mixed-phase photocatalysts. The smaller size of the TiO_2 particles and subsequent higher surface are together with the so-called synergetic effect between anatase and rutile are arguments that support the observed ordering of the photocatalytic activity. The addition of Ru to An sample leads to a decrease in photocatalytic activity, suggesting the absence of a synergetic effect due to the co-presence of anatase and rutile in the photocatalyst. Ohno et al. [7] reported, for the photocatalytic oxidation of naphtaline, that an artificial mixture of anatase and rutile had a better photocatalytic activity than the pure anatase and rutile phases alone. These results, obtained for the naphtaline oxidation, are contradictory to our results that showed that a physical mixture of anatase and rutile phase is not beneficial for the oxidation of 4-CP. On the contrary, Ohtani et al. [4] showed that there was no synergetic effect in a "reconstructed" P25 photocatalyst for the acetic acid photocatalytic oxidation, as we observed in this study for the 4-CP oxidation. It is important to note that these authors have checked activities for several photocatalytic reaction systems, while the results of the present work are only valid for this photocatalytic reaction system. More precisely, these authors have isolated "pure" anatase and

rutile particles from P25 (by selective etching) and then different phase compositions were used as photocatalysts in the oxidation of acetic acid in aerated solutions. In this last work, addition of rutile to anatase had no positive effect on the photocatalytic activity, indicating the absence of any synergetic effect. In addition, it has been suggested that post-treatment of isolated anatase and rutile produced a change of their photocatalytic activities. Thus, our results support the idea that the so-called synergetic effect might not operate in all the photocatalytic oxidation processes used for the degradation of organic pollutants from aqueous effluents.

4. Conclusions

In this study we consider the influence of the mixing ratio in anatase to rutile physical mixtures on the photocatalytic degradation of 4-chlorophenol from aqueous solution. For this purpose, we used TiO_2 Degussa P25, "pure" anatase and "pure" rutile commercial powders as starting materials. Anatase and rutile were isolated as pure phases by selective dissolution in H_2O_2/NH_4OH and in 10% HF, respectively. All TiO_2 samples were thoroughly characterized by various techniques. The crystalline phases of photocatalysts were confirmed by X-ray diffraction and Raman spectroscopy. TEM images revealed that anatase particle have a spherical-shaped morphology while rutile particles are mainly rod-shaped with larger sizes.

Band gap energy (E_g) has been firstly calculated by using the classical Tauc-plot method and it has been observed that the values obtained are comparable with other reported in literature. A more accurate method for the calculation of the band gap energies, based on the use of the first derivative curves of the DR–UV–vis spectra, was also proposed.

The removal efficiencies of 4-chlorophenol from aqueous effluents, as a measure of the photocatalytic activity, indicate that Degussa P25 is the most active photocatalyst, followed closely by pure anatase samples. There is virtually no difference between the two pure anatase samples, in spite of the differences observed in the physical–chemical properties of these materials. At the other extremity, pure rutile photocatalysts displayed a lower efficiency in the oxidation of 4-CP, with almost no difference between the commercial and the separated sample. The photocatalytic activities of the physical mixtures of An and Ru improve as the anatase increases. Adding rutile to anatase does not lead to an improvement of the photocatalytic activity in the oxidation of 4-chlorophenol from water. The results seem to disprove the existence of a synergetic effect of anatase and rutile phases, at least in this particular photocatalytic system.

Acknowledgments

This work was supported by the Romanian National Authority for Scientific Research, CNCS-UEFISCDI, project number PN-II-PT-PCCA-2011-1491 and CNCSIS-UEFISCSU project number PN-II-IDEI code 368/2008. The authors acknowledge also the support of EURODOC Project "Doctoral Scholarships for research performance at European level" POSDRU/88/1.5/S/59410, (ID59410) financed by the European Social Found and Romanian Government.

References

[1] M. Pelaez, N.T. Nolan, S.C. Pillai, M.K. Seery, P. Falaras, A.G. Kontos, P.S.M. Dunlop, J.W.J. Hamilton, J.A. Byrne, K. O'Shea, M.H. Entezari, D.D. Dionysiou, Appl. Catal., B: Environ. 125 (2012) 331–349.
[2] J.M. Herrmann, Appl. Catal., B: Environ. 99 (2010) 461–468.
[3] H. Kazuhito, I. Hiroshi, F. Akira, Jpn. J. Appl. Phys. 44 (2005) 8269–8285.
[4] B. Ohtani, O.O. Prieto-Mahaney, D. Li, R. Abe, J. Photochem. Photobiol. A 216 (2010) 179–182.
[5] M. Batzill, E.H. Morales, U. Diebold, Phys. Rev. Lett. 96 (2006) 026103.
[6] D.C. Hurum, A.G. Agrios, K.A. Gray, T. Rajh, M.C. Thurnauer, J. Phys. Chem. B 107 (2003) 4545–4549.
[7] T. Ohno, K. Sarukawa, K. Tokieda, M. Matsumura, J. Catal. 203 (2001) 82–86.
[8] T. Ohno, K. Tokieda, S. Higashida, M. Matsumura, Appl. Catal., A: Gen. 244 (2003) 383–391.
[9] V. Loddo, G. Marci, L. Palmisano, A. Sclafani, Mater. Chem. Phys. 53 (1998) 217–224.
[10] T. Ohno, K. Sarukawa, M. Matsumura, J. Phys. Chem. B 105 (2001) 2417–2420.
[11] B. Ohtani, Y. Azuma, D. Li, T. Ihara, R. Abe, Trans. Mater. Res. Soc. Jpn. 32 (2) (2007) 401–404.
[12] C. Catrinescu, D. Arsene, P. Apopei, C. Teodosiu, Appl. Clay Sci. 58 (2012) 96–101.
[13] M. Pera-Titus, V. García-Molina, M.A. Baños, J. Giménez, S. Esplugas, Appl. Catal., B: Environ. 47 (2004) 219–256.
[14] A. Bojinova, R. Kralchevska, I. Poulios, C. Dushkin, Mater. Chem. Phys. 106 (2007) 187–192.
[15] H. Kominami, H. Kumamoto, Y. Kera, B. Ohtani, J. Photochem. Photobiol., A 160 (2003) 99–104.
[16] O. Carp, C.L. Huisman, A. Reller, Prog. Solid State Chem. 32 (2004) 33–177.
[17] K. Demeestere, J. Dewulf, H. Van Langemhove, B. Sercu, Chem. Eng. Sci. 58 (2003) 2255–2267.
[18] K. Okimura, Surf. Coat. Technol. 135 (2001) 286–290.
[19] M. Bonne, S. Pronier, Y. Batonneau, F. Can, X. Courtois, S. Royer, P. Marecot, D. Duprez, J. Mater. Chem. 20 (2010) 9205–9214.
[20] P. Kubelka, J. Opt. Soc. Am. 28 (1948) 448–457.
[21] A.B. Murphy, Sol. Energy Mater. Sol. Cells 91 (2007) 1326–1337.
[22] A. Beltran, L. Gracia, J. Andres, J. Phys. Chem. B 110 (2006) 23417.
[23] A.H. Dorian, C.S. Charles, J. Mater. Sci. 46 (2011) 855–874.
[24] N. Serpone, J. Phys. Chem. B 110 (2006) 24287.
[25] B. Ohtani, J. Photochem. Photobiol., C 11 (2010) 157–178.
[26] G.L. Chiarello, E. Selli, L. Forni, Appl. Catal., B: Environ. 84 (2008) 332–339.